Techno-economic optimization of a packed-bed for utility-scale energy storage

B. Cárdenas[a]*, T.R. Davenne[a], J.Wang[b], Y.Ding[c], Y.Jin[d], H.Chen[e], Y.Wu[f], S.D. Garvey[a]

[a] Dept. of Mechanical, Materials and Manufacturing Engineering, University of Nottingham, United Kingdom
[b] School of Engineering, University of Warwick, Coventry, United Kingdom
[c] Birmingham Centre for Energy Storage, University of Birmingham, Birmingham, United Kingdom
[d] Global Energy Interconnection Research Institute, Beijing China
[e] Institute of Engineering Thermophysics, Chinese Academy of Sciences, Beijing, China
[f] Laboratory of Enhanced Heat Transfer and Energy Conservation, Beijing University of Technology, Beijing, China

Corresponding author's email: Bruno.Cardenas@nottingham.ac.uk

Abstract

The optimization of a packed bed for utility-scale applications is presented in this paper. The effects that particle size, aspect ratio and storage mass have on the roundtrip exergy efficiency of the store are thoroughly analysed. The paper seeks to provide a clear insight of what ranges of values for the aforementioned design parameters are adequate to consider when designing a grid-scale packed bed. Simulations were carried out using a one-dimensional model that accounts for temperature-dependent properties and self-discharge losses. The assumed operating temperature range for the packed bed is 290-823 K, which is typical of CSP plants and CAES systems. A 24-hour work cycle (12 hr charge / 12 hr discharge) with variable power (10 MW peak) and a total energy storage requirement of 79.4 MWh_{th} has been considered for the study.
It has been found that exergy losses are minimized if a configuration based on an aspect ratio between 0.5 and 0.8 is adopted and the size of the rocks is finely tuned for the specific shape of container. In this work—unlike similar studies—a cost-benefit analysis has been carried out, which indicates that increasing the thermal storage mass leads to a considerable increase in efficiency. A mass overrating of 50% yields the lowest levelized cost of storage for the economic scenario considered. The optimum design obtained from the optimization process has an aspect ratio of 0.6, a particle size of 4mm and a mass overrating factor of 1.5. This packed bed attained a roundtrip exergy efficiency of 98.24 %

Keywords
CAES; aspect ratio; mass overrating factor; thermal energy storage; exergy efficiency; levelized cost of storage

1 Introduction

Thermal energy storage (TES) technologies are deemed as a very flexible, promising and economically attractive solution to the increasingly challenging problem of the time mismatch between periods of energy availability and demand created by the introduction of renewable-based generation to the grid [1].

There is a wide range of approaches, materials and configurations that have been studied by many authors. A broad overview on the state of the art of high temperature TES technologies is provided in [2-4]. Packed beds are a type of passive TES that store energy as sensible heat. These type of thermal stores have received great interest due to the high efficiencies attainable, low cost and overall simplicity for being used in CSP plants to decouple electricity production from solar irradiation periods and within compressed air energy storage (A-CAES) systems, which are used for balancing the power fed into the grid by other renewable sources, such as wind [5-7].

Some of the main features or advantages of packed beds are the following: (1) the storage material (commonly rocks) is abundant and economical. (2) Different types of heat transfer fluids (HTF) can be used, such as: molten salts, synthetic oils or air. (3) They can be used over a very broad temperature range; the upper temperature limit being the melting point of the rocks employed (~1200 K). (4) A direct heat transfer between the HTF and the storage material is possible. However, if the HTF is pressurized it may be more cost-effective to adopt an indirect charging/discharging scheme via an intermediate heat exchanger. (5) There is practically no degradation or chemical instability of the storage medium, especially if the HTF used is air. (6) Reduced capital cost due to the use of a single container in comparison to the two-tank system used in CSP plants.

The TES unit used in an energy storage or power generation plant is a key component as it influences directly the efficiency and cost effectiveness of the system. Consequently, special attention should be paid to their design. A vast amount of research has been devoted to develop accurate analytical models for simulating the behaviour and performance of packed beds under different work cycles, which allows studying the effect that different geometrical and operational have on the performance of the storage unit. Following, a review of some relevant literature is presented.

Bayón and Rojas [8] developed a single phase one-dimensional model for characterizing the behaviour of thermocline tanks with an effective storage medium formed by a liquid (molten salt, thermal oil or water) and a packed-bed (rocks or sand). The model considers losses to the environment, axial heat conduction and temperature independent properties of the materials. The authors present guideline plots for designing thermocline stores with maximum efficiency at various temperature intervals. Thermal power was found to be a critical parameter because the larger the power the higher the degree of freedom for choosing tank dimensions.

Nomenclature

Acronyms

A-CAES	Adiabatic compressed air energy storage
CAPEX	Capital expenditure
CSP	Concentrated solar power
HTF	Heat transfer fluid
LCOS	Levelized cost of storage
TES	Thermal energy storage

Sub-indices

0	Ambient conditions
c	Container
g	Gas
p	Particle
r	Rocks

Symbology

α	Individual aspect ratio
A	Mean cross sectional area (m^2)
β	Overall aspect ratio
Bi	Biot number
$\dot{B}_g$	Exergy content of the air stream (W)
B_{in}	Total exergy input during work cycle (J)
B_{l-Ex}	Exhaust exergy losses (J)
B_{l-HT}	Exergy losses due to heat transfer (J)
B_{out}	Total exergy output during work cycle (J)
B_{l-PD}	Exergy losses due to pressure drops (J)
B_{l-SD}	Exergy losses due to self-discharge (J)
C_p	Specific heat capacity (J/kg·K)
δt	Duration of time step (s)
δx	Height of a slice of geometry (m)
ΔB_r	Change in exergy content of packed bed (J)
ΔP	Pressure drop (Pa)
D_p	Particle diameter (m)
ε	Void fraction
E	Energy storage requirement (MWh_{th})
f	Friction factor
g	Gravitational acceleration (m/s^2)
η	Roundtrip exergy efficiency
h	Convection heat transfer coefficient ($W/m^2 \cdot K$)
H	Height of the packed bed (m)
k	Thermal conductivity (W/m·K)
λ	Component of total cost ($)
L	Lithostatic pressure of bed of rocks (Pa)
μ	Dynamic viscosity (Pa·s)
m	Mass (kg)
m_g	Mass flow rate of air (kg/s)
Nu	Nusselt number
Ø	Diameter of container (m)
ρ	Density (kg/m^3)
ψ	Value of total exergy input throughout lifespan ($)
Pr	Prandtl Number
P	Pressure (Pa)
Q_a	Heat transferred by advection (J)
Q_{conv}	Heat transferred by convection (J)
Q_k	Heat transferred by conduction (J)
r	Radius of container (m)
R	Air specific gas constant (J/kg·K)
Re	Reynolds number
s	Surface area (m^2)
S	Allowable stress of structural steel (Pa)
τ	Wall thickness (m)
t	Time (s)
T	Temperature (K)
v_g	Superficial velocity (m/s)
V	Volume (m^3)
ω	Number of cycles operated during lifespan
W	Work cycle
x	Number of slices in the geometry
z	Cost per unit of exergy ($/MWh)

Modi and Pérez [9] investigated the effect of the type of heat transfer fluid (molten salts and thermal oils), the storage temperature difference and the cycle cut-off criterion on the performance of the system. The study was carried out using a 1-D two-phase model that considered thermal losses from the lateral walls, neglected axial conduction and used temperature dependent properties only for the fluid phase. The authors pointed out that two important aspects for assessing the performance of the system are the cyclic behaviour and the time required to attain equilibrium conditions, which are highly sensitive not only to the storage temperature difference, but also to the cut-off temperature difference.

Van Lew et al. [10,11] developed a simplified 1-D two-phase model that employs constant fluid (thermal oil) and solid (granite rocks) properties and assumes null heat losses for investigating the effect of different parameters such as container aspect ratio, particle size, and void fraction on performance. The authors found that for the particular scenario studied the efficiency of the store increases as the aspect ratio increases (with a constant storage volume). Additionally, the efficiency decreases as the void fraction increases, reaching a minimum at 0.7. The energy storage efficiency decreases with the increase in the average diameter of rocks as a greater heat transfer resistance is encountered.

Xu et al [12, 13] investigated the effects of the type and size of rocks on the temperature distribution of a packed bed with molten salt as HTF. The study was based on a transient 2-D model with the following considerations: thermal losses from the lateral walls of the container, constant rock properties, temperature dependent properties of the HTF and more importantly, the temperature distribution within the solid particles is accounted for. Five storage materials (quartzite rock, ceramics, concrete, alumina and cast iron) were evaluated. The results show that increasing the particle diameter reduces heat transfer rate between solid particles and molten salt (due to particles limited thermal conductivity), which decreases the efficiency. However, it was found that the efficiency of the store is nearly independent from the properties of the solid material if the particle size is small enough.

Yang and Garimella [14,15] investigated the effect of particle diameter (quartzite rock), tank dimensions and mass flow rate of the HTF (molten salt) on the performance of a packed bed. The researchers developed a 1-D two-phase model that considered no heat losses to the surroundings, constant rock properties with no axial conduction and temperature dependent properties for the HTF. The authors reported that the storage efficiency increases with tank height and decreases as Reynolds number increases. Additionally, it was found that

smaller filler particles can greatly increase the discharge efficiency. For instance, a thermocline storage unit (2 MW, 5 MWh and Ø = 5 m) with a particle size of 50 mm has a discharge efficiency that exceeds by 12.9% that of a store with a particle size of 100 mm.

The great majority of the studies on packed beds of an industrial relevant scale that are available in the literature have been carried out considering molten salts or thermal oil as heat transfer fluids, given that those are the most commonly used HTF in CSP plants. Most of the models developed could be applicable to other heat transfer fluids, with due considerations and changes in properties. Nevertheless, some studies on packed beds that consider air as the HTF for being used in next-generation CSP plants and A-CAES systems have been realized.

Hänchen et al. [16] presented the analysis of a high temperature packed bed (steatite, rock, aluminium and steel) with air as HTF. The 1-D two-phase model developed considers conduction and convection inside the container, uniform temperature within the particles, thermal losses through the walls and constant properties for the solid material. The study showed that smaller particle sizes lead to higher overall efficiencies (notwithstanding pumping work increases significantly) due to the sharper temperature front obtained. Additionally, it was noted that increasing the mass flow rate and reducing the container height leads to markedly higher outlet temperatures during the charge.

Anderson et al. [17,18] proposed a simplified one-equation thermal model for the behaviour of a packed bed with alumina spheres as the storage medium and air as HTF. The model considers temperature dependent properties for both phases and assumes thermal equilibrium between the solid and fluid phases. The researchers reported a good agreement between the temperature predictions from the model and experimental measurements. It is highlighted that the model developed is only valid in cases where the heat capacity and thermal conductivity of the solid medium are high with respect to those of the fluid.

Zanganeh et al. formulated a two-phase dynamic numerical model for a packed bed with air as the HTF that considers variable thermo-physical properties for both phases. [19,20]. Subsequently the authors carried out a parametric study on the design of a 7.2 GWh_{th} packed bed (mix of quartzite, limestone and sandstone) for a CSP plant (8hr-charge/ 16hr-discharge) with aims at understanding the impact of design parameters (such as particle size) on thermal losses, pumping power, discharge temperature and overall storage efficiency [21]. It is pointed out that there are no general design rules for packed beds. Each unit must be optimized for performance (efficiency, outflow temperature profile) and costs (thermal losses, pumping work, and materials costs) given the requirements (capacity, charging and discharging duration, mass flow rate and temperature).

Opitz and Treffinger [22] developed a lumped element model with a two-phase formulation for the modelling of a packed bed. Steatite and steel were evaluated as storage materials while air and flue gas were used as HTFs. The model accounts for the variation on the void fraction with radial position. Heat transfer through the wall as well as radial and axial conduction in the solid phase are considered. The scheme adopted by the authors allows the implementation of the model in object oriented modelling environments (such as Modelica), which offers the possibility of integrating it within bigger plant models.

Mertens et al [23] carried out an optimization of an 18.6 MWh_{th} quartzite packed bed for a CSP power plant that utilizes air as the HTF. A 1-D two phase model that accounts for losses through the wall, non-spherical particles and change of void fraction with particle size was used. The authors found that—within the range of values explored—a packed bed with an aspect ratio of 0.75 and a particle size of 0.5 mm attained the highest thermal efficiency (97.4%); however it is remarked that a full-system optimization is important as well since the packed bed design deemed as the optimum from a thermal performance point of view might not lead to an optimum overall electric efficiency of the plant due to other operational parameters such as the cut-off temperature of the steam generator .

Klein et al [24, 25] proposed a pressurised packed bed of alumina spheres that uses air as the HTF. The transient model developed considers all relevant heat transfer mechanisms and was experimentally validated for the temperature range of 350-900 °C. The model was used to conduct a parametric study of a 1.55MWh_{th} TES unit with a volume of 7m^3 to be used with a micro gas turbine. The design obtained achieved an efficiency of 78% with an aspect ratio of 4 and 110 mm diameter particles. Similarly, Agalit et al. [26] proposed a 1-D two-phase model that considers radiative heat transfer between the solid particles (quartzite rocks and asbestos-ceramic) as well as between the particles and the container's wall. The authors analysed two high temperature packed beds to be used in hybrid solar power plants that operate in the temperature ranges of 1200-800 °C and 653-350 °C, reporting that overall storage efficiencies of up to 94% are achievable.

1.1 Objectives

A considerable amount of research has been devoted in recent years to the study of packed beds for energy storage applications, as the literature review shows. Parametric studies aimed at understanding the effect that different design and operational parameters (particle size, void fraction, mass flow rates, charging/ discharging times, materials used, etc.) have on the performance of the TES units have been carried out by numerous authors; however there are some important aspects that still have not been formally studied.

i) There are no parametric studies in the literature where the thermal storage mass is treated as a variable, despite it is widely known that a larger mass (for the same duty) will improve the efficiency of a TES unit.

ii) Although the effect of the shape of the container has been discussed in the literature there is no clear guidance available with respect to what is a good value (or range of values) to consider for the aspect ratio when designing a packed bed. The present work seeks to fill this gap.

In this paper the optimization of a packed bed for an A-CAES system is presented. The study is aimed at understanding the

effect that aspect ratio, particle size and storage mass have on the exergy losses of the store. A simple cost model is included which allows analysing the trade-off between efficiency and the cost per unit of exergy storage capacity of the packed bed.

The results of the optimization work carried out are presented in terms of exergy and exergy losses rather than energy. The rationale behind this is rather simple: Electricity is 100% exergy whereas heat has some exergy only, the amount depends on the temperature. In other words 1 J of heat is not equivalent to 1 J of electricity; therefore if a packed bed can store 1 MWh of heat, the amount of electricity that it can take in and store is much less, ~500 kWh. Expressing losses, storage capacity and efficiency in terms of exergy allows a quicker understanding of the real capacity of the unit and enables a much more straightforward comparison with other storage technologies, such as electrical batteries.

2 Optimization process

There is a virtually endless array of designs that a packed bed sized for a certain load may take. For example, a thin and tall packed bed (α>1) may be desirable because exergy losses due to self-discharge (heat conducted down the thermal front) are reduced—or slowed down—due to a smaller cross-sectional area and a greater separation between the hot and cold ends of the store; however the container will have a greater surface area and more insulation will be required. This kind of configuration is particularly attractive for locations where space is limited and maintaining a small footprint is crucial.

On the other hand, a short and wide design (α<1) has the advantage of a lower pumping load due to the reduced height and larger cross-sectional area of the container. A further benefit of a small α is a lower cost for the container and thermal insulation required. The minimum wall thickness required reduces considerably with the height of the packed bed while the surface area of the container reaches a minimum at an α=1; both of these parameters are good indicators of cost.

Figure 1 shows the algorithm followed in the optimization process. Several different mass overrating factors (β) are studied ($1.0 \leq \beta \leq 3.0$), for each one of which a range of aspect ratios are evaluated ($0.2 \leq \alpha \leq 1.5$). Additionally, for every design of packed bed (combination of α and β) an optimum size of rock is determined. Small particles provide a large surface area thus heat transfer losses are reduced but entail increased pressure drops across the store.

It is recognized that the optimum design for a certain duty may not be optimal for different operating conditions; notwithstanding, the results from this parametric study will provide a solid reference of what are the appropriate ranges to consider for each variable (α & β) when designing a utility-scale packed bed and what are the effects on performance and cost of shifting the design of the store towards smaller or larger values.

3 Mathematical modelling

A transient 1-D two-phase model has been developed to simulate the charging and discharging of a packed bed and evaluate its performance. The model is based on a discretised explicit scheme that allows its implementation in numerical solvers (such as Matlab). Among the assumptions and simplifications made by the model it is worth highlighting: (1) Temperature dependent physical properties are used for both materials. (2) A temperature gradient in the radial direction is not considered. (3) A uniform temperature within the solid particles is assumed. (4) A 1-D Newtonian plug flow for the HTF is assumed. (5) Geometric properties are assumed to be constant throughout the packed bed. (6) Heat conduction down the thermal front is considered in both materials. (7) Heat losses through the wall are neglected as well as all heat transfer by radiation.

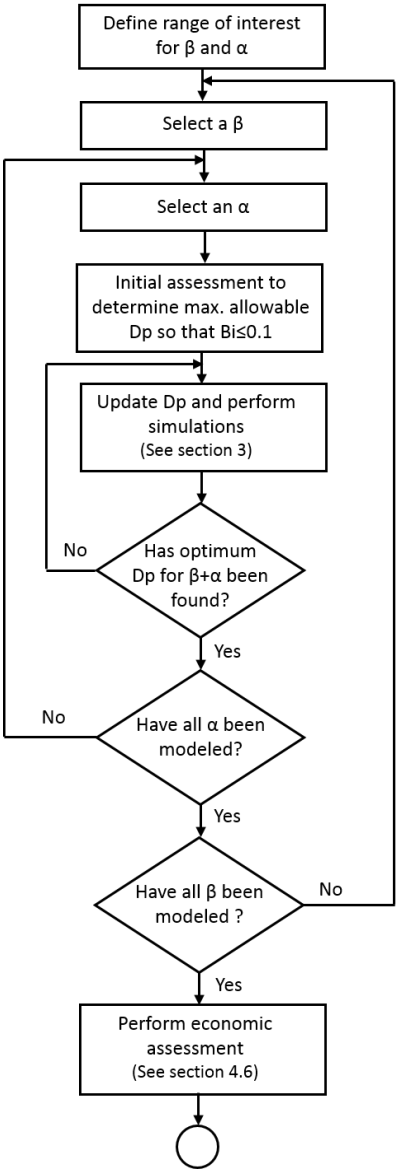

Figure 1. Algorithm of the optimization process

The process followed by the calculation algorithm is explained graphically by Figure 2. The work cycle (represented by a time dependent function) to which the TES unit will be subjected is analysed to determine the duty of the store. The packed bed is sized accordingly

The total mass of rock (m_r) required is calculated through Eq. (1), where E is the amount of heat to be stored by the packed bed (dictated by the work cycle) and C_{p-r} is the specific heat capacity of the rocks. The factor β is known as the mass overrating factor. This scaling factor—as its name suggests—allows increasing the mass of rocks used in the store whereby an improvement in performance can be achieved. A β equal to

one yields the absolute minimum mass of rock required for storing the energy contained in the work cycle.

$$m_r = \beta \cdot \frac{E}{C_{p-r} \cdot \Delta T} \quad (1)$$

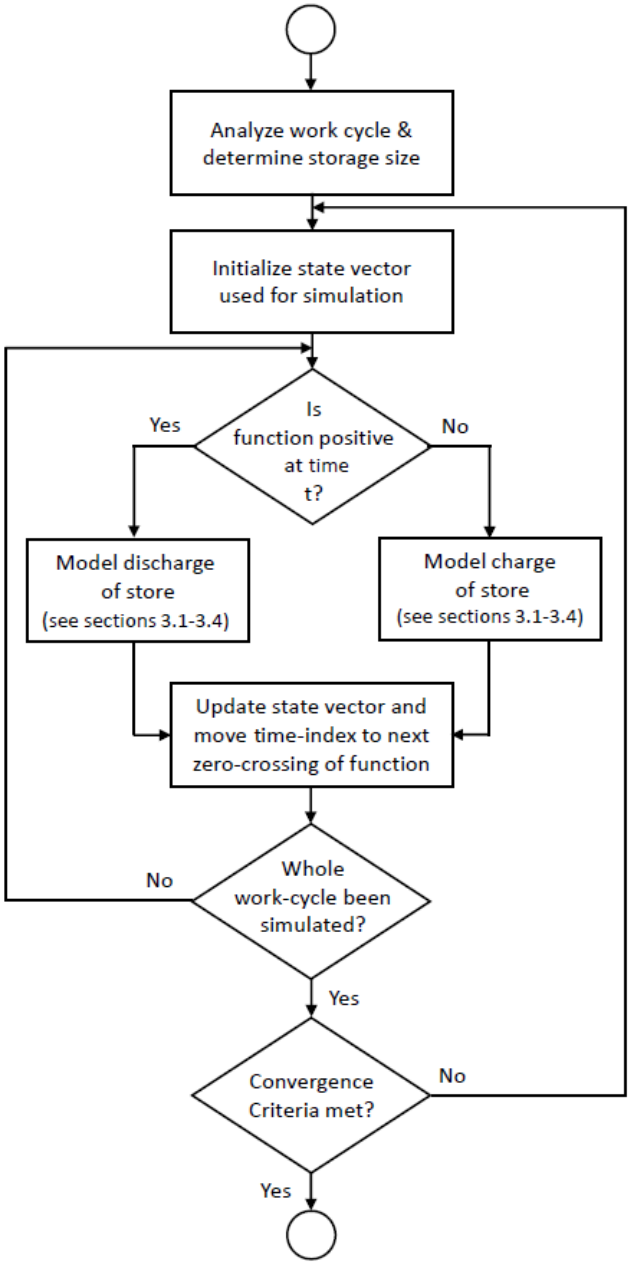

Figure 2. Algorithm for the modelling

The operating temperatures considered for the packed bed are 823 and 290 K for the hot and cold ends respectively, which are typical operation temperatures in CSP plants [27] and high temperature A-CAES systems [28]. The steel used for the container provides an additional storage capacity; however it is very small compared to the thermal mass of the rocks and it is almost never accounted for. In this study the thermal capacity of the container is neglected.

Once the storage mass has been determined, the geometry of the packed bed can be characterized. A number of geometric parameters such as the volume of the container (based on the void fraction (ε) and the density of the rocks (ρ_r)) and its shape (dictated by α) are calculated at this stage, together with the size of the rocks.

Several different particle sizes are evaluated to determine the optimum one for a given shape of container. The maximum allowable particle size is established based on the criterion that a Biot number greater than 0.1 (maximum value for assuming a constant temperature within the rock particles) should not be observed at any one section of the packed bed at any time during the work cycle.

A state vector containing information of the temperatures of the two materials (rock and air) in each of the *x* slices of the geometry and the different components of exergy loss is initialized. The algorithm moves forward in time through the work-cycle function simulating —as appropriate— the charge or discharge of the packed bed. A very important aspect of the simulation is that convergence is checked once a full work cycle has been concluded. Several work cycles are simulated until the convergence criteria is met, in this way it is ensured that the initial conditions assumed in the first run do not have an effect in the results obtained. The convergence criteria in place are two ratios: The first is a ratio between the exergy content of the packed bed at the end and at the start of the work cycle. The second is a comparison of the exergy loses at the end of the current work cycle and at the end of the previous work cycle. These ratios should have a value of 1, however due to numerical inaccuracies this is never the case. A tolerance of ± 0.01% is used.

The following subsections (3.1-3.3) describe the calculations that take place as the algorithm progresses in time through the work-cycle. The calculations can be classified in 3 groups: 1) determination of pressure drops and flow characteristics, 2) heat transfer calculations (which are the core of the simulation) and 3) the calculation of the different components of exergy loss.

3.1 Determination of flow characteristics

As aforementioned, the model simulates the charging (or discharging) of a packed bed as a load is passed through it. Once the load at a specific time has been translated into a mass flow of air ($\dot{m}_g$), the pressure drops along the height of the packed bed and the flow characteristics are determined.

The inlet pressure required for the air to leave exit the packed bed at ambient pressure is calculated in an iterative way. In other words, the inlet pressure is only marginally higher than ambient in order to sustain flow and overcome friction with the rocks.

A vector of initial guesses for the pressure (P) at each slice is created. Based on this vector the density (ρ) of the air at each of the slices is determined through Eq. (2).The superficial flow speed of the air (υ_g) can be subsequently calculated by means of Eq. (3), where A_c is the total cross-sectional area of the container. Even though a part of the cross sectional area of the container is occupied by rocks, the velocity is calculated as if air was flowing freely. The "packed-bed-specific" Reynolds and Ergun equations (Eq. (4) and (6), respectively) account for this.

$$\rho_g = \frac{P}{R \cdot T_g} \quad (2)$$

$$v_g = \frac{\dot{m}_g}{\rho_g * A_c} \tag{3}$$

The Reynolds number for flow through a packed bed is given by Eq. (4) [29], where μ is the dynamic viscosity of the fluid and D_p is the particle diameter, defined by Eq. (5) [30]. In the case of this study, the particles are considered to be perfectly spherical, whereby Eq. (5) is reduced to 2*r.

$$Re = \frac{\rho_g \cdot v_g * D_p}{\mu} \tag{4}$$

$$D_p = \left(\frac{6}{\pi} \cdot V_p\right)^{1/3} \tag{5}$$

The air flow is obstructed by the rocks inside the container, which generates friction and results in a loss of pressure. The pressure drops (ΔP) across each of the slices of the geometry can be calculated by means of Eq. (6) [31], where δx is the height of the slice, f is the friction factor given by Eq. (7) [32] and ε is the void fraction (space not occupied by rocks).

$$\Delta P = \frac{f \cdot \delta x \cdot \rho_g \cdot {v_g}^2 \cdot (1-\varepsilon)}{2 \cdot D_p \cdot \varepsilon^3} \tag{6}$$

$$f = 258(1-\varepsilon) \cdot Re^{-1} + 4.36 \cdot \left(\frac{2}{3} \cdot \frac{Re}{1-\varepsilon}\right)^{-0.12} \tag{7}$$

Typically the friction factor is calculated through the experimental correlation proposed by Ergun [33]; however several authors have reported that it is only accurate for a very limited range of Reynolds numbers [34-38].

The vector of pressures across the height of the packed bed is subsequently updated by adding the accumulated pressure drops calculated through Equation (6). The iterative loop is repeated until the variation in the vector of pressures is negligible. After this, the heat transfer coefficient (h) can be calculated by means of Eq. (8) where k_g is the thermal conductivity of the gas. The Nusselt (Nu) and Prandtl (Pr) numbers are given by Eqs. (9) and (10), respectively [39].

$$h = Nu \cdot k_g \cdot {D_P}^{-1} \tag{8}$$

$$Nu = 2.0 + 1.1 Pr^{1/3} \cdot [Re \cdot (1-\varepsilon)]^{3/5} \tag{9}$$

$$Pr = \mu \cdot C_{pg} \cdot {k_g}^{-1} \tag{10}$$

3.2 Heat transfer calculations

Thermal calculations are expressed in a discretised explicit form. In every slice of the geometry there is an elemental volume of rock whose mass and surface area are the sum of the individual masses and surface areas of all the rock particles in that slice. Likewise, there is an elemental volume of air which occupies the void space in the slice. It is assumed that the temperatures and properties of both elements, rock and air, are uniform throughout the volume of the slice.

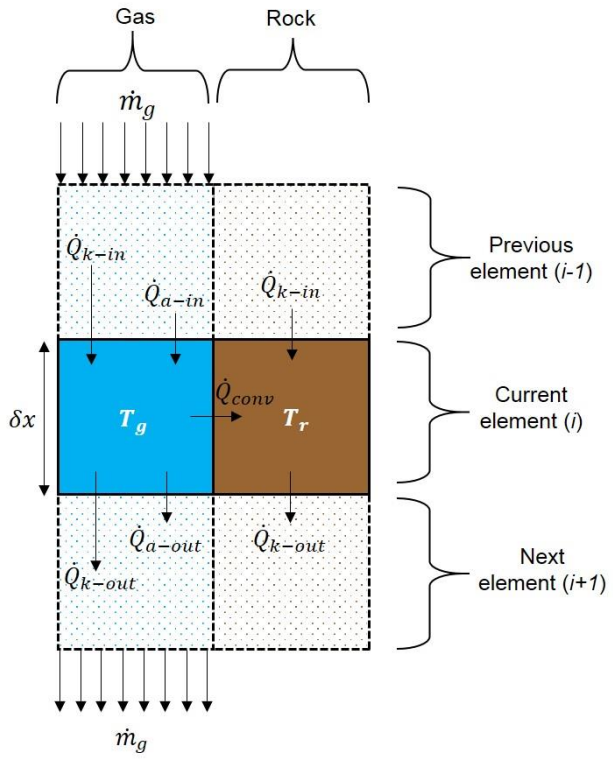

Figure 3. One-dimensional finite element model of packed bed showing gas and solid elements and their interactions

The heat transfer model is created considering the energy balance of the elemental volume of gas contained in a slice i of the geometry, as Figure 3 shows. As it can be observed, the change of energy within the gas is equal to the net heat flow by advection ($Q_{a-in} - Q_{a-out}$) plus the net heat flow by conduction ($Q_{k-in} - Q_{k-out}$) minus the heat transferred by convection to the element of rock in a charging period (Q_{conv}). The above can be expressed mathematically through Eq. (11), in which the indices i and j represent the position in space and time, respectively.

$$\rho_g C_{pg} A_c \varepsilon \delta x \left(T_g^{(i,j+1)} - T_g^{(i,j)}\right) = \ldots \\ \ldots (Q_{a-in} - Q_{a-out}) + (Q_{k-in} - Q_{k-out}) - Q_{conv} \tag{11}$$

Where:

$$Q_{a-in} = \dot{m}_g C_{pg} \left(\frac{T_g^{(i-1,j)} + T_g^{(i,j)}}{2}\right) \delta t \tag{12}$$

$$Q_{a-out} = \dot{m}_g C_{pg} \left(\frac{T_g^{(i+1,j)} + T_g^{(i,j)}}{2}\right) \delta t \tag{13}$$

$$Q_{k-in} = k_g A_g \left(\frac{T_g^{(i-1,j)} - T_g^{(i,j)}}{\delta x}\right) \delta t \tag{14}$$

$$Q_{k-out} = k_g A_g \left(\frac{T_g^{(i,j)} - T_g^{(i+1,j)}}{\delta x}\right) \delta t \tag{15}$$

$$Q_{conv} = hs_r \left(T_g^{(i,j)} - T_s^{(i,j)}\right) \delta t \tag{16}$$

The rate of change of the temperature of the gas at time j, can then be expressed as Eq. (17):

$$\frac{\delta T_g}{\delta t} = \frac{Q_1 + Q_2 - Q_{conv}}{\rho_g C_{pg} A_c \varepsilon \delta x} \quad (17)$$

Where:

$$Q_1 = \frac{\dot{m}_g C_{pg}}{2}\left(T_g^{(i-1,j)} - T_g^{(i+1,j)}\right) \quad (18)$$

$$Q_2 = k_g A_g \left(\frac{T_g^{(i-1,j)} - 2T_g^{(i,j)} + T_g^{(i+1,j)}}{\delta x}\right) \quad (19)$$

Similarly, the change of energy in the element of rocks can be calculated by means of Eq. (20):

$$m_r C_{pr}\left(T_r^{(i,j+1)} - T_r^{(i,j)}\right) = (Q_{k-in} - Q_{k-out}) + Q_{conv} \quad (20)$$

Where:

$$Q_{k-in} = k_r A_r \left(\frac{T_r^{(i-1,j)} - T_r^{(i,j)}}{\delta x}\right)\delta t \quad (21)$$

$$Q_{k-out} = k_r A_r \left(\frac{T_r^{(i,j)} - T_r^{(i+1,j)}}{\delta x}\right)\delta t \quad (22)$$

The rate of change of the temperature of the rocks is given by Eq. (23), which allows updating the temperatures after each time-step taken.

$$\frac{\delta T_r}{\delta t} = \frac{Q_1 + hs_r\left(T_g^{(i,j)} - T_r^{(i,j)}\right)}{m_r C_{pr}} \quad (23)$$

Where:

$$Q_1 = k_r A_r \left(\frac{T_r^{(i-1,j)} - 2T_r^{(i,j)} + T_r^{(i+1,j)}}{\delta x}\right) \quad (24)$$

3.3 Mechanisms of exergy loss

The exergy content of the air at the inlet of the packed bed during the charge as well as the exergy of the air at the outlet during the discharge can be calculated by means of Eq. (25):

$$\dot{B}_g = \dot{m}_g \left[\int_{T_0}^{T} C_{pg} dT - T_0\left(\int_{T_0}^{T} C_{Pg}\frac{dT}{T} - R\int_{P_0}^{P}\frac{dP}{P}\right)\right] \quad (25)$$

During a charging phase air enters the packed bed through the hot end at the nominal inlet temperature (823 K) and at a pressure marginally higher than ambient (to compensate for pressure drops). Conversely, during a discharge phase, air flows into the packed bed through the cold end at ambient temperature whereby it has a rather small exergy content due exclusively to the inlet pressure.

It is noteworthy that the same discretised explicit calculation approach can be used for modelling the operation of cold stores, which are used among other applications in pumped thermal energy storage systems (PTES) [40]. In a cold packed bed the same heat transfer processes occur but the direction of the gas flow is reversed. During the charge, air at very low temperatures (~120K) enters the packed through the bottom side and removes energy from the rocks, which increases the exergy stored. During the discharge phase, air at ambient temperature enters the packed bed through the top side and is cooled by the rocks, which extracts the exergy stored [41].

The model considers four mechanisms of exergy loss: 1) exergy losses due to heat transfer, 2) exhaust losses, 3) exergy losses due to pressure drops and 4) exergy losses due to self-discharge. It should be noted that exergy losses due to the dissipation of heat into the surroundings of the packed bed are not considered.

The exergy losses owing to pressure drops (B_{l-PD}) can be calculated from the pressure drops in each slice of the geometry through Eq. (26):

$$B_{l-PD} = \sum_{i=1}^{x} -\dot{m}_g \cdot T_0 \cdot R \cdot ln\left(\frac{P^{(i+1,j)}}{P^{(i,j)}}\right) \quad (26)$$

As the packed bed approaches a full charge, increasingly hotter gas will start to emerge from the cold end of the container, which represents an exergy loss. This form of exergy loss is known as "exhaust losses" (B_{l-Ex}) and can equally be calculated via Eq. (25). These losses only occur during the charging phase.

Exergy losses due to self-discharge (B_{l-SD}) are caused by the heat that is conducted down the temperature gradient within the thermal front. These losses are always present, during both phases of operation and even when the packed bed is in a purely storage mode. Self-discharge losses dictate (together with losses to the surroundings) how long the exergy can be stored in a thermocline-based store. These losses can be calculated through Eq. (27)

$$B_{l-SD} = \sum_{i=1}^{x-1} Q_{kg}\left(\frac{T_0}{T_g^{(i+1,j)}} - \frac{T_0}{T_g^{(i,j)}}\right) + Q_{kr}\left(\frac{T_0}{T_r^{(i+1,j)}} - \frac{T_0}{T_r^{(i,j)}}\right) \quad (27)$$

The exergy losses due to heat transfer (B_{l-HT}) refer to the losses caused by the convective heat transfer from the air to the rocks (or viceversa during discharge) and the losses due to the advective heat transfer inherent to the flow of the gas along the height of the packed bed. In most cases, these losses are the largest source of exergy loss and can be calculated through an exergy balance, as shown by Eq. (28):

$$B_{in} = B_{out} + \Delta B_r + B_{l-PD} + B_{l-Ex} + B_{l-SD+} + B_{l-HT} \quad (28)$$

During a charging phase there is no output of exergy (B_{out}) while during a discharge phase there are no exhaust losses (B_{l-Ex}) and the input of exergy (B_{in}) is minimal, only to compensate for the losses due to pressure drops (B_{l-PD}).

3.4 Thermo-physical properties

The mathematical model developed considers temperature dependent properties for both materials. Air is used as the HTF, since the packed beds modelled are envisioned to work within a high temperature A-CAES system. The temperature dependent functions for dynamic viscosity, thermal

conductivity and specific heat capacity of air proposed by Lemmon and Jacobsen [42] and Lemmon et al. [43] have been adopted. It should be mentioned that these functions are valid over a wide range of pressures (0.1 – 100+ MPa). In the case studied, the air stream is considered to be "non-pressurized" having only a marginally-higher-than-ambient pressure to sustain flow. The rocks used in the model are basalt, an igneous rock commonly considered as a sensible heat storage medium. A constant density of 2650 kg/m^3 is assumed [44, 45] while the temperature dependent functions for thermal conductivity and specific heat capacity are based on experimental data reported by Hartlieb et al [46].

Polynomial expressions, in the form of Eq. (29), were fitted to the data found in the literature. Tables 1 and 2 provide the coefficients for the temperature dependent properties of air and rocks, respectively. It should be mentioned that these equations are valid for a temperature range between 290 and 850 K.

$$f(T) = AT^4 + BT^3 + CT^2 + DT + E \quad (29)$$

Table 1. Coefficients for the temperature dependent functions of different physical properties of air.

	μ (Pa·s)	**k_g** (W/m·K)	**C_{pg}** (J/kg·K)
A	0	0	0
B	0	0	-4.16x10^{-7}
C	-5.038x10^{-13}	1.172x10^{-9}	8.611x10^{-4}
D	1.736x10^{-9}	1.277x10^{-5}	-0.3679
E	1.133x10^{-7}	-1.05x10^{-3}	1049

Table 2. Coefficients for the temperature dependent properties of basalt rock.

	k_r (W/m·K)	**C_{pr}** (J/kg·K)
A	1.86x10^{-14}	-2.038x10^{-10}
B	7.41x10^{-10}	1.479x10^{-6}
C	-2.10x10^{-6}	3.076x10^{-3}
D	1.524x10^{-3}	2.709
E	1.274	191.3

4 Results obtained and discussion

4.1 Effects of storage mass, aspect ratio and particle size on the total exergy losses

The work cycle (W) considered in the modelling is a sine wave with a peak amplitude of 10 MW and period of 1 day ($0s < t < 86400s$), described by Eq. (30):

$$W = -10 \cdot \sin\left(\frac{2 \cdot t \cdot \pi}{86400}\right) \quad (30)$$

In the work cycle considered, there is only 1 charge period ($0s < t < 43200s$) and 1 discharge period ($43200s < t < 86400s$). The cycle demands an energy storage capacity (E) of 76.4 MWh$_{th}$, which are supplied to the store by a stream of air at 823 K. With basis on this value a mass of 566.5 x10^3 kg of rock was calculated as the minimum mass required for servicing the load ($\beta=1$).

The outcomes of this study are transferrable to other applications with different work cycles that consider non-sinusoidal profiles. The optimum combination of parameters (β, α and D_p) will change but the results found here will still be a good reference and serve as an adequate initial guess for the optimization process. One of the cases where the design of the packed bed will change dramatically is when the packed bed is intended for long term storage; or in other words if there is a prolonged period of inactivity between the charging and discharging phases. In such case the self-discharge exergy losses will become the main form of exergy loss and the design of the packed bed will be tuned accordingly to try to minimize them.

In a practical application it is rarely desirable to allow the thermal front to move all the way down to the cold end of the store because increasingly hotter air will emerge from the container, which translates directly into exergy losses. A mass overrating factor (β) higher than 1 can be used to mitigate this problem.

The optimization carried out comprises three parameters: mass overrating factor, aspect ratio and the particle size. Different combinations of β and α are evaluated. For every design explored (β+ α) an optimum size of rocks is determined. The parameters used for the modelling of the packed bed subjected to the work cycle described above are summarized in Table 3.

Table 3. Parameters used in the modelling

	Parameter	**Value**	**Units**
Operational / Design	T_0	290	K
	T inlet (charge)	823	K
	T inlet (discharge)	290	K
	P_0	101325	Pa
	P inlet (charge/discharge)	See Eq.(6)	Pa
	Work cycle	See Eq.(30)	MW
	Min. mass of rock	566.5x10^3	kg
	Mass Overrating	1.0 to 3.0	--
	Aspect ratio	0.2 to 1.5	--
	Void fraction	0.3954	--
	Particle Size	0.5 to 20	mm
Physical Properties	Air properties	See Table 1	--
	Rock properties	See Table 2	--
	Rock Density	2650	kg/m^3
Model Setup	No. of Elements (Slices)	200	--
	Convergence Criterion 1	>0.9999 <1.0001	--
	Convergence Criterion 2	>0.9999 <1.0001	--
	Tolerance of ODE Solver	1x10^{-7}	--

The void fraction is a very important parameter that influences the performance of the packed bed [10,11]; however in practical applications is hard to control as it depends on the arrangement of the particles. In this paper the rocks are

considered to be perfectly spherical, although Eq. (5) allows accounting for any non-sphericity. When spheres of the same size are used, void fractions between 0.66 and 0.2595 can be achieved. Random packing of spheres attains on average a void fraction of 0.36. An hexagonal packing of the spheres, which achieves a void fraction of 0.3954 [47] is assumed for this study. The results obtained using this value are conservative given that when spheres are packed randomly (as it would be done in a real life application) a higher density is achieved. It should be noted that greater packing densities can be achieved when particles of different diameters are used. It is also important to remark that the void fraction remains constant even when the particle size changes.

Figures 4 and 5 show the first stage of the optimization process. For every aspect ratio in the range $0.2 \leq \alpha \leq 1.5$ the diameter of the rocks is varied to find the particle size that yields the lowest total exergy losses. Figure 4 shows the results obtained for β=1.5 while Figure 5 presents the results for β=2.0. For clarity, only the curves for 4 values of α are shown in each plot. The total exergy losses shown in the figures are the sum of the four forms of exergy loss previously described. The total exergy losses can also be calculated as the difference between the exergy input during the charging period and the exergy output during the discharge phase.

It can be seen in Figures 4 and 5 that at smaller aspect ratios the size of the particles has a much more marked effect on the exergy losses, whereas at large aspect ratios (α>1) curves flatten out and a wider range of particle sizes achieve a very similar performance.

Regardless of the aspect ratio of the packed bed, the total exergy losses follow a similar trend. As the diameter of the rocks increases the losses start to decrease until reaching a minimum at the optimum particle size. This is because very small particles produce significant pressure losses. As the size of the rocks increases past the optimum size, the total exergy losses start increasing as well due to the effect of heat transfer and exhaust losses. Large particles do not allow an effective heat transfer along the height of the packed bed, which is mainly owed to a reduced surface area to volume ratio.

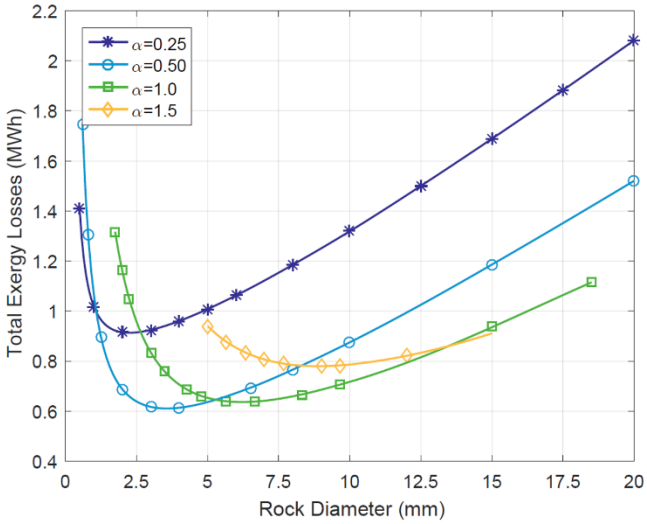

Figure 4. Determination of the optimum particle size for different values of α for a β=1.5

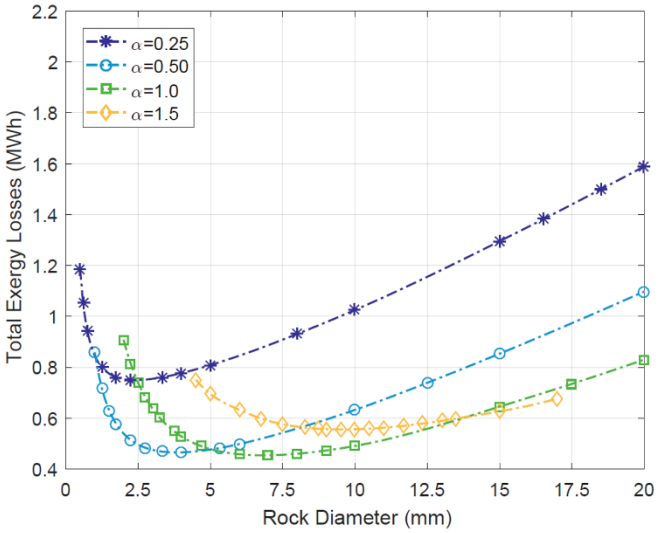

Figure 5. Determination of the optimum particle size for different values of α for a β=2.0

It can also be observed that smaller α's require smaller particle sizes to achieve the best performance (minimum losses), despite having a container with a larger diameter. For example, the losses of a packed bed with a β=1.5 and an α=0.25 are at a minimum when the diameter of the rocks is 2.24 mm, while the losses of a design with the same β and an α=1.5 reach a minimum with a particle size of 8.91 mm. For comparison, a packed bed with a β=2.0 and an α= 0.25 exhibits the best performance when the diameter of the rocks is 2.38 mm while with an α=1.5 the optimum diameter of the rocks increases to 9.52 mm.

The behaviour of the total exergy losses of a packed bed as the values for the mass overrating factor (β) and the aspect ratio (α) change is shown in Figure 6. In the figure, the exergy losses for every combination of α and β are the minimum exergy losses for that particular design, achieved through the fine tuning of the particle size. It can be seen that the performance of a packed bed improves considerably as more storage mass is used (i.e. a larger β).

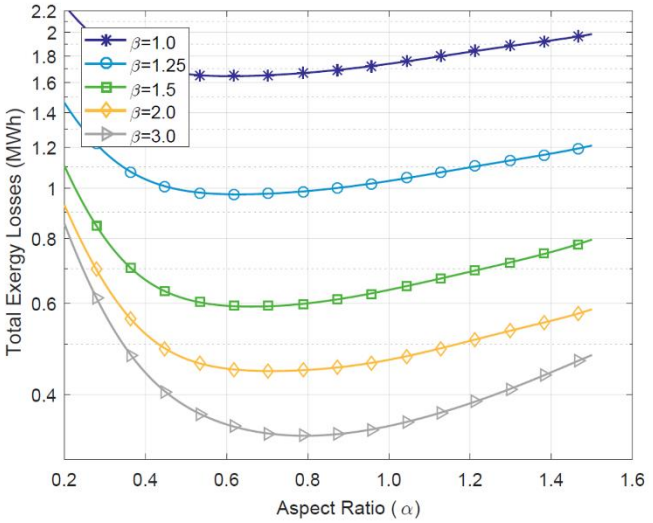

Figure 6. Behaviour of the total exergy losses of a packed bed as the aspect ratio varies.

The four different types of exergy loss (heat transfer, exhaust, pressure drops and self-discharge) reduce as the value of β increases. For example, exergy losses due to heat transfer

decrease thanks to an increase in the available heat transfer area while exergy losses due to pressure drops reduce due to a greater cross-sectional area of the container. The reasons for the improvement of each of the four mechanisms of exergy loss are discussed in further detail in subsections 4.2-4.5

It can also be seen in Figure 6 that for any given value of β, the exergy losses of the packed bed decrease as the α reduces until reaching a minimum between $0.5 \leq \alpha \leq 0.8$, below which they rise again. The increase of exergy losses for α's smaller than the optimum is owed primarily to self-discharge losses which increase dramatically as the height of the container is reduced, bringing the hot and cold ends of the packed bed closer together. This phenomenon will be explained in depth in subsection 4.5.

Another interesting detail worth noting is that the optimum aspect ratio does not remain constant from one value of β to another. For example, a packed bed with a β=1 reaches an optimum at an α=0.6, while a packed bed with a β=3 exhibits the lowest losses with an α=0.8. The roundtrip exergy efficiency of the former configuration is 95.07 %, while the latter attains an efficiency of 99%. As mentioned in section 3, the model does not take into account losses to the environment. It should be highlighted that only discrete values for α were evaluated in the study despite that α is in reality a continuous variable. Therefore the best values shown are a close approximation to the optimum rather than a true optimum.

The results presented in Figure 6 suggest that large values of β should be employed to improve the performance of the store. However, the improvement in performance becomes increasingly smaller as the mass overrating factor (β) becomes larger. Therefore at some point, the performance gains will not justify the additional capital expenditure. This study focuses primarily on values of β between 1.5 and 2, which are deemed (from an economic point of view) as reasonable levels of mass overrating for practical applications. Subsection 4.6 shows that the optimum value for β lies within this range.

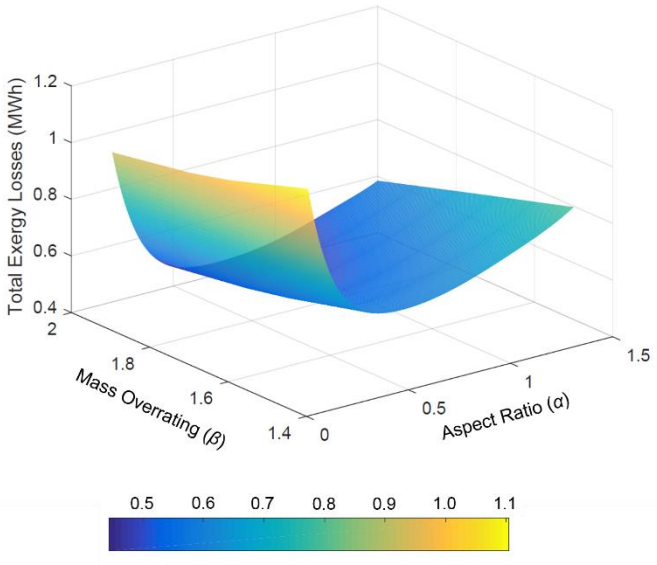

Figure 7. Effect of the mass overrating factor (β) and aspect ratio (α) on the exergy losses of a packed bed

With aims at providing a better perspective of the improvement in performance as the mass of the thermal store increases, Figure 7 shows (in the form of a surface plot) the behaviour of the total exergy losses over a work cycle for designs considering a $1.5 \leq \beta \leq 2.0$ and a wide range of α.

Figures 8 and 9 show the contribution of the different mechanisms of exergy loss to the total exergy losses of different designs of packed beds for a β=1.5 and 2.0, respectively. The behaviour of each of the four types of exergy loss will be analysed in depth in sections 4.2 to 4.5. Nevertheless, it can be seen that regardless of the value of β, at small α's self-discharge losses are the major contributor of loss while at large α's losses due to pressure drops become critical.

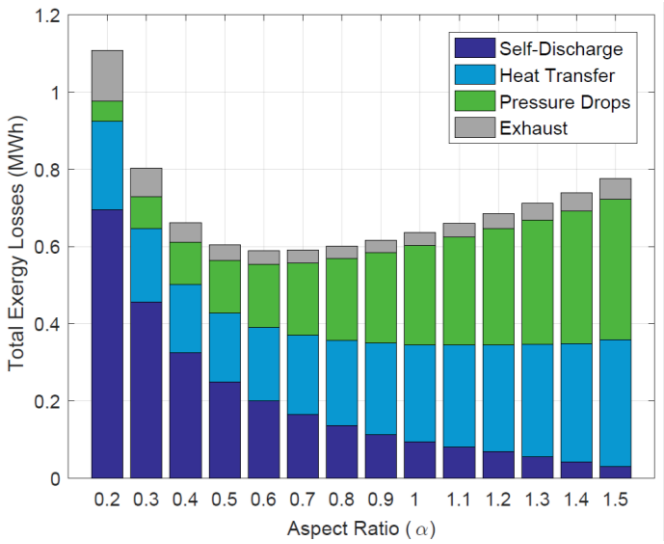

Figure 8. Distribution of the total exergy losses of packed beds with a β=1.5 into the different mechanisms of loss.

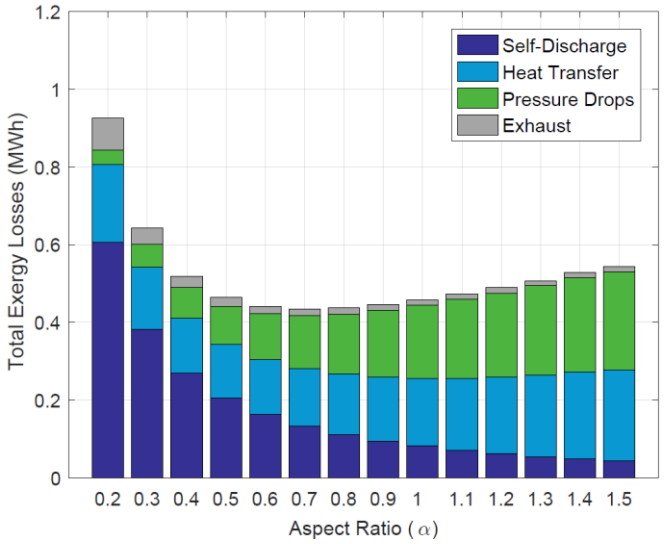

Figure 9. Distribution of the total exergy losses of packed beds with a β=2.0 into the different mechanisms of loss.

Figure 10 shows the evolution of the thermal front throughout a full work cycle for a packed bed with an α=0.6 and 4mm diameter rocks. This configuration attained the lowest losses among designs based on a β=1.5, having an exergy efficiency of 98.24%. It can be seen that at the end of the charging period (12^{th} hour) the cold end (height=0) has a temperature well above ambient (346.94 K), which as aforementioned, contributes to the exergy losses of the store. Moreover, due to the irreversibilities present during the charge and discharge periods, the packed bed is not able to sustain its nominal output

temperature of 823 K for the entire 12 hours of discharge. At the end of the discharge period, the hot end has a temperature of 753.49 K.

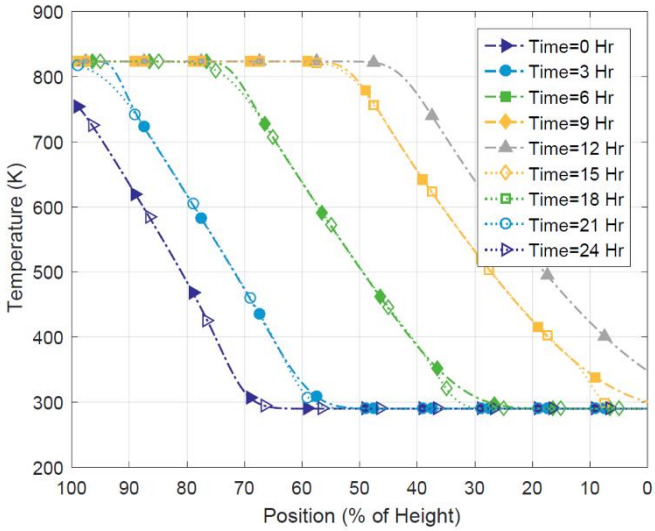

Figure 10. Evolution of the thermal front (rocks) within a packed bed with a β=1.5, α=0.6 and a 4mm particle size.

In the following subsections the behaviour of each of the four mechanisms of exergy loss as the particle size is optimized for a given set of α and β will be thoroughly discussed.

4.2 Behaviour of the exergy losses due to heat transfer

Figure 11 shows the exergy losses due to heat transfer for packed beds with a β=1.5 (solid lines) and 2.0 (dashed lines). For any given values of α and β the exergy losses due to heat transfer behave almost linearly as the particle size varies, being smaller when small diameters of rock are used due to an increase in the total heat transfer surface of the packed bed.

For reference, a packed bed based on a β=1.5 has 300 m^2 of heat transfer area per m^3 of rocks when a rock diameter of 20mm is used, which increases to 1200 m^2/m^3 when a rock diameter of 5mm is used. The available heat transfer area is only a function of the total mass and size of the rocks and does not depend on the aspect ratio of the packed bed.

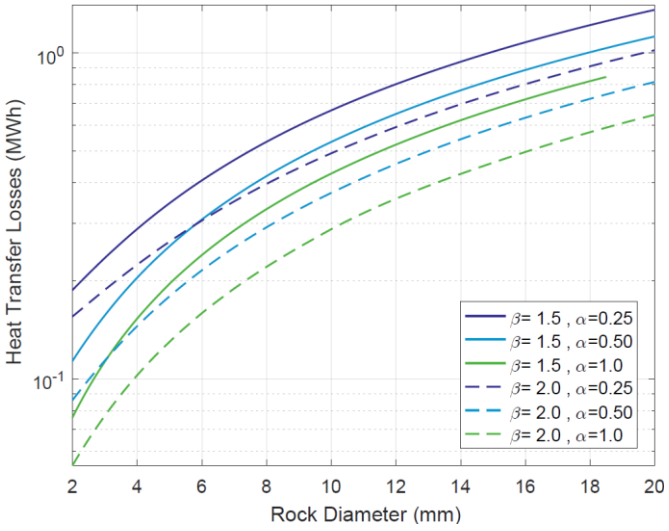

Figure 11. Behaviour of exergy losses due to heat transfer as the particle size varies

The range for the particle size was determined based on the Biot number (ratio of the heat transfer resistances inside of and at the surface of the rocks), which is proportional to the diameter of the rocks. The largest particle size considered in the study does not exceed a Biot of 0.1, which is the limit for considering a constant temperature inside each particle. If larger rocks were to be used, an additional form of exergy loss would need to be introduced to account for the heat transfer from the surface of the rocks to their core and vice versa. For Biot numbers <0.1 this exergy loss is negligible.

When a larger β is used, the total surface area of the packed bed increases (even if the particle size stays the same) because a larger amount of rocks are in the container. This increase in the ratio of total surface area per unit of exergy transfer produces a considerable reduction of the heat transfer losses.

Furthermore, Figure 11 shows that heat transfer losses decrease for increasing α's, which can be explained by means of Figure 12. The height of the packed bed (namely the separation between the hot and cold ends) plays an important role in defining the shape of the thermal front. Greater heights lead to sharper fronts, although several other factors have an influence on this. The packed bed with an α=1.0 has a sharper front (with a steeper slope) in comparison to a design with an α=0.25, so at the end of the charging period (12th hour) the temperature of its cold end is lower than in the design with a smaller aspect ratio.

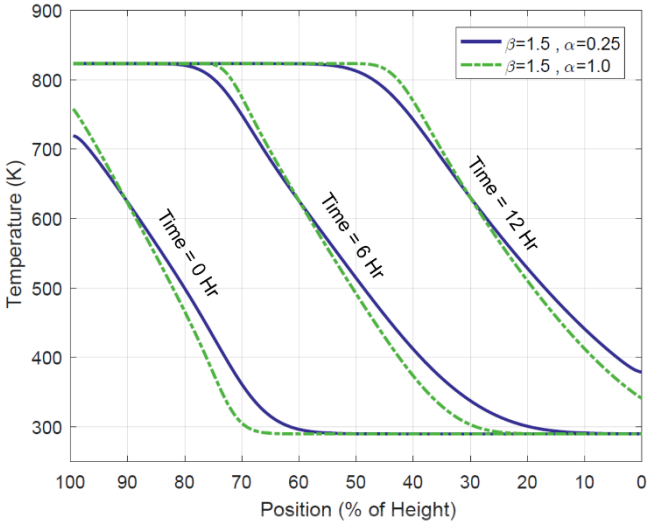

Figure 12. Thermal front at different times of the work cycle of different design of packed beds with a β=1.5

This rise of the temperature of the cold end has a strong impact on the performance of the thermal store. Besides causing exhaust losses due to the air leaving the packed bed with some heat content left, a high temperature in the cold end at the end of the charging period generates substantial heat transfer losses during the subsequent discharge period because air at ambient temperature (290 K) is pumped through the cold end of the packed bed, where it will come in contact with rocks at a much higher temperature (~379 K for an α=0.25), hence heat is transferred across a big temperature difference and exergy is destroyed.

At the end of the discharge, due to irreversibilities in the process, the packed bed with an α=0.25 has a lower temperature at its hot end in comparison with design based on

an α=1.0. This will cause further heat transfer losses during the following charging cycle when air at the nominal inlet temperature of 823 K is pumped through the hot end of the store and encounters rocks ~100 K colder.

4.3 Behaviour of the exhaust exergy losses

Figure 13 shows the behaviour of the exhaust losses for designs based on different values of β and α as the particle size changes. Two sets of curves can be identified, solid and dotted lines. The solid lines represent a β=1.5 while the dotted lines represent a β=2.0; each colour represents a different α.

Exhaust losses are directly proportional—similarly to heat transfer losses—to the diameter of the rocks. The total heat transfer area increases for smaller particle sizes, therefore the air stream has less exergy remaining in it upon exiting the packed bed at the cold end.

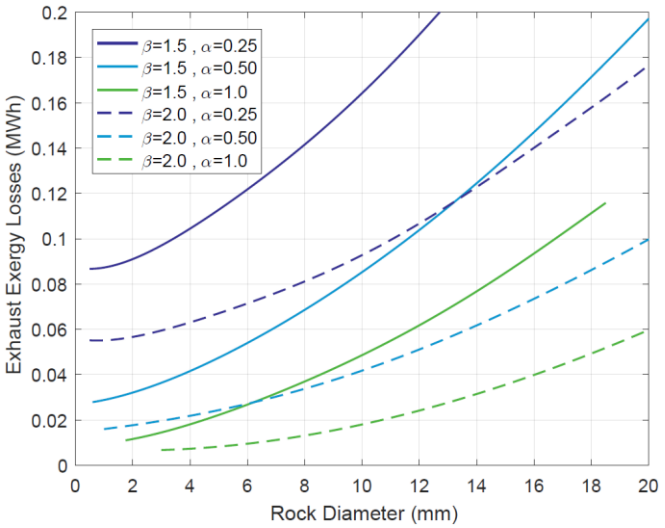

Figure 13. Behaviour of exhaust exergy losses for designs based on different α and β as the particle size varies

It can be seen that for any given size of rocks, exhaust losses reduce as α increases. As aforementioned, a greater separation between the hot and cold ends of the packed bed (consequence of a larger α) helps to achieve a steeper thermal front (as shown in Figure 12) which in turn causes the air to leave the store at a lower temperature. For instance, a packed bed with a β=1.5 and α=0.25 has 0.1415 MWh of exhaust losses when rocks of 8 mm of diameter are used, while these losses reduce to 0.037 MWh if α increases to 1.0, keeping β and the rock size constant. In Figure 13 it can also be seen that exhaust losses decrease as the mass overrating factor increases.

Figure 14 provides further insight on the behaviour of the exhaust losses. In the figure, the temperature profiles of the cold end of different designs of packed beds (β=1 with different α and sizes of rocks) throughout the work cycle are shown.

It can be seen that at the end of the charging period (12th hour), designs with a low aspect ratio (solid lines) have a much higher temperature at their cold end in comparison to designs with a large aspect ratio (dashed lines), which explains the increased exhaust exergy losses. For example, the cold end of a packed bed considering a β=1, α=0.25 and 6mm rocks reaches a temperature of 379.07 K in contrast with a packed bed based on an α=1.0, whose cold end's temperature rises only up to 341.32 K.

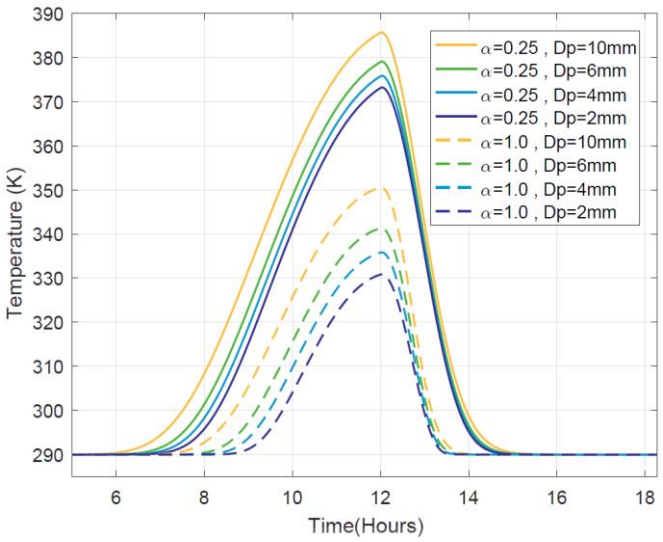

Figure 14. Temperature profile of the cold end of different designs of packed beds throughout a full work cycle

For the same aspect ratio, smaller rocks yield lower temperatures at the end of the charging period due to an increased heat transfer area, which is in agreement with the behaviour depicted in Figure 13. Additionally, it may be observed that the cold end temperatures of designs with a small α start to increase earlier, i.e. large aspect ratios are capable of maintaining the temperature of the cold end at near ambient (which is desirable) for a longer period.

4.4 Behaviour of the exergy losses due to pressure drops

Pressure drops, as shown in Figures 8 and 9, become a major contributor to the total exergy losses of the packed bed as the aspect ratio increases. Figure 15 shows the behaviour of the exergy losses caused by the pressure drops in the storage unit. In the figure, four different groups (colours) of curves can be identified, each one of these groups represents a different aspect ratio. For each aspect ratio, 3 different values of β (solid, dashed and dotted lines) are plotted.

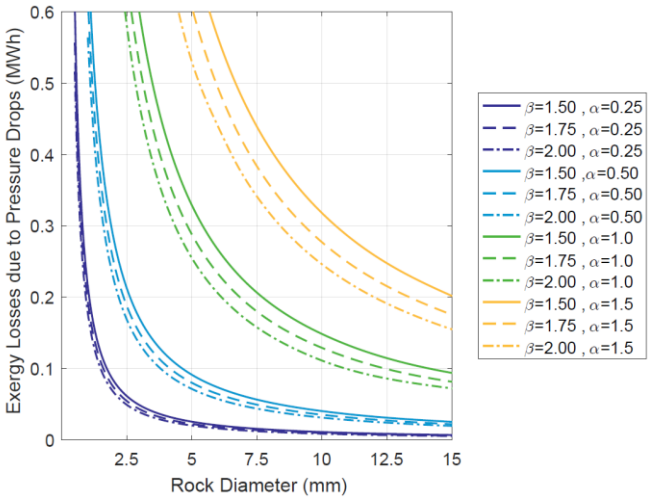

Figure 15. Exergy losses due to pressure drops in the packed bed for designs with different α, β and sizes of rock.

For any given combination of α and β, exergy losses due to pressure drops increase exponentially as the size of the rocks decreases because the stream of air faces a higher resistance against flow. Regardless of the particle size, packed beds with larger values of α have much higher exergy losses due to pressure drops. For example, considering a rock diameter of 8mm, a design based on a β=1.5 and α=0.25 has 0.0144 MWh of exergy losses due to pressure drops during a full work cycle, while these losses increase to 0.0523, 0.1917 and 0.4084 MWh for values of α of 0.5, 1.0 and 1.5, respectively. The foregoing is due to two factors: the height of the bed increases and the cross-sectional area of the container reduces, which entails an increase in the velocity of the air and consequently in the pressure drops, as Eq. (3) and (6) indicate.

Pressure drops reduce for increasing values of β—as expected—because as the container of the packed bed grows the mass flow to cross-sectional area ratio (mass-flux) reduces. The effect in the pressure drops of increasing β is more notorious at large aspect ratios, where the cross-section available is rather small for the air flow.

4.5 Behaviour of the self-discharge exergy losses

Figure 16 shows the behaviour of the exergy losses due to the self-discharge of the packed bed as different mass overrating factors, aspect ratios and rock sizes are used. In the figure, four groups of curves (different colours) can be identified. Each group represents a different α and comprises 3 curves (different line styles), each of which represents a different β.

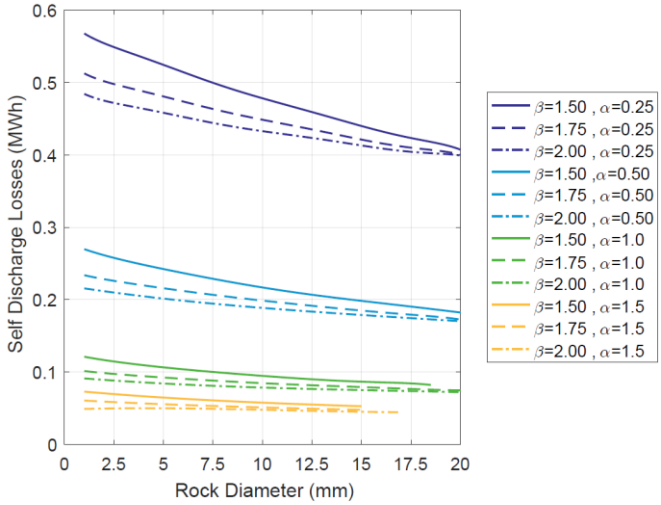

Figure 16. Exergy losses due to self-discharge of the packed bed or designs with different α, β and sizes of rock.

It can be seen that self–discharge losses increase significantly as the aspect ratio decreases. As α shifts towards smaller values, the length between the hot and cold ends reduces and the cross–section increases, which facilitates the conduction of heat down the thermal front. For a β= 1.5 and a rock diameter of 5 mm, a packed bed with an α=1.5 has 0.065 MWh of exergy losses due to self-discharge in the course of a work cycle, while a design based on an α=0.25 loses 0.524 MWh.

Similar to the other forms of exergy loss discussed in the previous subsections, for any given value of α self-discharge losses reduce as β increases because the separation between the hot and cold ends of the packed bed lengthens. In designs based on a small aspect ratio self-discharge losses become a major source of exergy loss, overshadowing in some cases the improvement observed in the other forms of loss. It is precisely due to the effect of self-discharge losses that below a certain aspect ratio (~0.6, depending on β) the total losses of the packed bed start to increase again instead of continuing to diminish, as Figure 6 shows.

Many studies neglect this form of exergy loss, which may be acceptable for aspect ratios greater than 1. However, an optimization study cannot be properly carried out without taking these losses into consideration because the resultant function describing the efficiency of the packed bed would be a monotonic curve indicating the optimum is found at a very small aspect ratio (α<<0.5) when this is not necessarily the case.

4.6 Cost-benefit analysis

Subsections 4.1-4.5 have amply demonstrated that for the duty and scale of packed beds this study is concerned with, a very sizeable reduction in the total exergy losses can be attained through the optimization of the aspect ratio and the size of the rocks used. It has been found that designs based on an aspect ratio between $0.5 \leq \alpha \leq 0.8$ (depending on β) exhibit the lowest losses.

Besides a lower operational cost owed to the reduced exergy losses, a further benefit of adopting a configuration for a packed-bed based on a small aspect ratio is the reduction of some cost-driving parameters such as the container's surface area and wall thickness.

The minimum wall thickness (τ) of the cylindrical container to hold any one packed bed is determined, as shown in Eq. (31), by the radius of the container (which is a function of α), the lithostatic pressure exerted by the bulk of rocks (L) and the maximum hoop stress (S) the material of the construction can tolerate. Smaller aspect ratios entail smaller bed heights, which results in thinner container walls due to the reduced lithostatic pressure of the column of rocks.

If the packed bed was pressurized, the pressure of the air stream would also play an important role in determining the thickness of the container's wall. This paper considers a non-pressurized packed bed, which is charged/discharged by a stream of air with a pressure very slightly higher than ambient.

$$\tau = -\frac{L \cdot r_c}{L - 2 \cdot S} \tag{31}$$

Where:

$$L = \rho_r \cdot g \cdot H \tag{32}$$

$$r_c = \left(\frac{V_c}{2 \cdot \pi \cdot \alpha}\right)^{1/3} \tag{33}$$

The surface area of the container (s_c), unlike the wall thickness, is not monotonic for the range of α's analysed, reaching a minimum at α=1 (see Eq. (34)). Nevertheless, the volume of steel required for the construction of the container (given by the product of surface area and wall thickness) decreases continuously until α~0.3 (depending on value of β). Consequently, designs for packed beds based on a small aspect

ratio (α< 1) have a lower capital cost than those which consider an α>1, due to the reduced volume of steel required for their construction and a smaller area requiring insulation.

$$s_c = 2\pi \cdot \left(\frac{V_c}{2 \cdot \pi \cdot \alpha}\right)^{2/3} \cdot (1 + 2\alpha) \quad (34)$$

The overall results of the optimization process (presented in subsection 4.1) show that a reduction in the exergy losses can be achieved by increasing the mass of the packed bed by a certain factor (β) and suggest that a packed bed should be as big as possible to improve its efficiency. However; the factor by which the thermal mass of the store can be overrated is limited by economics. The improvement in performance becomes smaller for large values of β, which means that the cost of enlarging the store for a certain duty is not justified by the efficiency gained.

To illustrate this fact, a simple cost model has been developed. The cost of the packed bed (CAPEX) is defined as the sum of three components: the cost of the steel of the container (λ_{steel}), the cost of the insulation ($\lambda_{insulation}$) and the cost of the rocks (λ_{rocks}). It is worth highlighting that all three components of cost are influenced either directly or indirectly by the mass overrating factor.

$$CAPEX = \lambda_{steel} + \lambda_{insulation} + \lambda_{rocks} \quad (35)$$

Figure 17 shows the CAPEX calculated for different designs of packed beds. In designs with a β=1 the cost of the container represents 59.8-70.9% (depending on α) of the total cost, the cost of insulation accounts for 13.8-21.3% and the rocks contribute 15.2-19.6%. For comparison, in designs with a β=3, the total cost of the thermal store is distributed as follows: the container represents 71.8-80.2%, the insulation between 7.8-12.5% and the rocks account for 11.9-15.98%.

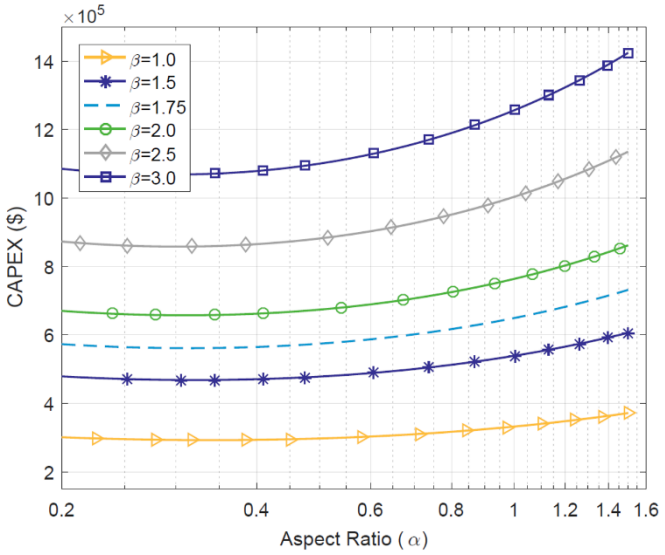

Figure 17. Variation in the CAPEX of the packed bed as different values for β and α are used.

The levelized cost of storage (LCOS), defined by Eq. (36), is used to find the optimum β, that is to say, the value of β that yields the lowest cost per unit of exergy stored ($/MWh). In the equation ψ_{in} represents the total value of the exergy that will be stored in the packed bed throughout its lifespan (ω) while B_{out} is the total exergy output of the store throughout its lifespan. Typically the LCOS metric considers other costs such as maintenance and depreciation. In this study they are neglected (for simplicity) since they can be assumed to be constant for every design of packed bed [48, 49].

$$LCOS = \frac{CAPEX + \psi in}{B_{out}} \quad (36)$$

Where:

$$\psi_{in} = B_{in} * \omega * z \quad (37)$$

$$B_{out} = B_{in} * \eta * \omega \quad (38)$$

It is clear that the LCOS is a trade-off between the total exergy losses and the CAPEX of the packed bed. Losses need to be minimized (i.e. efficiency improved) to increase the actual output of the store over time (B_{out}), but in doing so a penalty in CAPEX is paid. The parameters used for the cost-benefit analysis carried out are summarized in Table 4. It should be mentioned that the values are simply representative figures.

Table 4. Parameters considered in the cost-benefit study

	Parameter	Value	Units
Material properties	Insulation *k*	0.08	W/m-k
	Ambient *h*	10	W/m^{2}K
	Allowable energy losses per cycle	0.01*E	MWh
	Steel Allow. Stress	150	MPa
	Density Steel	8000	kg/m^3
Costs	Cost of steel	20	USD/kg
	Cost of insulation	264.5	USD/m^3
	Cost of rocks	0.1	USD/kg
	Value of exergy (z)	65	USD/MWh
Operational Parameters	Theoretical Output (B_{in})	33.392	MWh
	Lifespan of store	20	Years
	Number of cycles (ω)	7300	Cycles

Figures 18 and 19 show the LCOS achieved by a packed bed (under the specified work cycle in the specific economic scenario) as the design parameters α and β are varied.

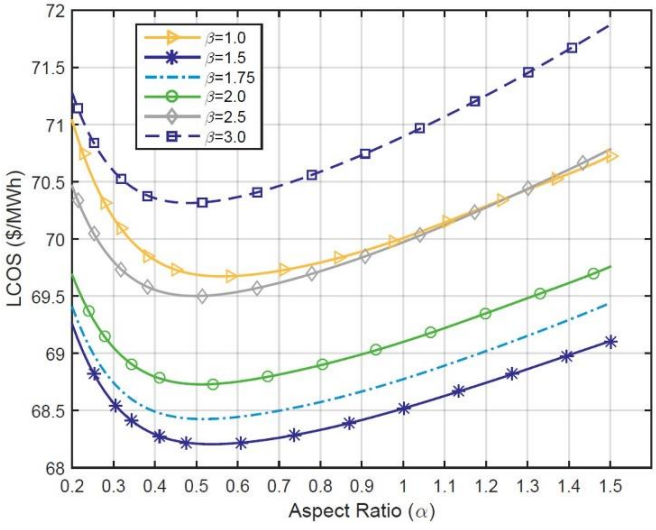

Fig 18. Variation in the LCOS of the packed bed as different values for β and α are used.

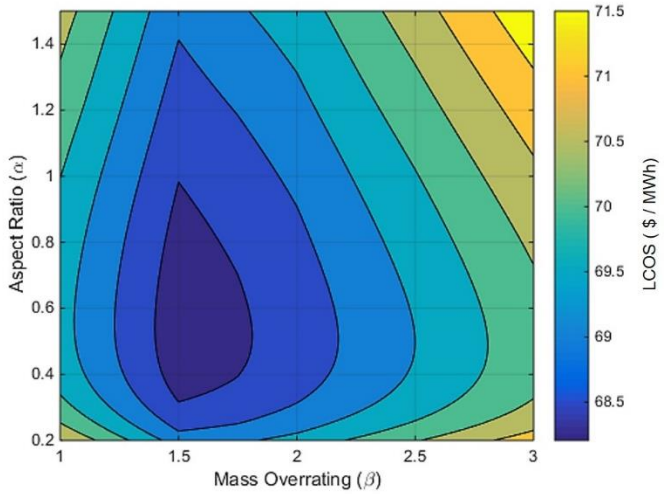

Figure 19. Determination of the optimum combination of β and α from an economic standpoint.

It can be seen that designs based on a β=3, yield the highest LCOS due to their elevated CAPEX, despite having the lowest losses. Analogously designs based on a β=1 yield high values of LCOS due to their high exergy losses, despite having a low CAPEX. The minimum LCOS is observed with a packed bed based on a β=1.5 and an α=0.6.

The geometrical, operational and performance parameters of the best performing configuration for a packed bed found after the techno-economic optimization process are summarized in Table 5.

Table 5. Parameters of the optimum design found

	Parameters	**Value**	**Units**
Geometrical	Overrating Factor (β)	1.5	--
	Mass of rock	849734.2	kg
	Volume of rock	320.65	m^3
	Void fraction	0.3954	--
	Particle Size	4.0	mm
	Total heat transfer area	1500	m^2/m^3
	Aspect Ratio (α)	0.6	--
	Container diameter	10.402	m
	Container height	6.241	m
	Container surface area	368.686	m^2
	Min. Wall thickness	5.632	mm
Operational	Max. Flow rate	17.98	kg/s
	Max. Inlet pressure	1.024	Bar
	Max. Air velocity	0.493	m/s
	Max. Heat transfer coeff.	77.923	W/m^2K
	Max. Biot number	0.034	--
	Total exergy input	33.558	MWh
	Temp. Hot end @24 hour	753.49	K
	Temp. Cold end @ 12 hour	346.94	K
	Ex. Losses due to heat transfer	188.71	kWh
	Ex. Losses due to pressure drops	166.8	kWh
	Exhaust exergy losses	33.102	kWh
	Ex. Losses due to self-discharge	201.056	kWh
	Roundtrip exergy efficiency	98.24	%

5 Concluding remarks

Packed beds have received a great deal of interest in recent years due to their high efficiencies, overall simplicity, relative low cost and potential to be used in very high temperature applications.

A comprehensive study of the effect of aspect ratio and particle size on the different mechanisms of exergy loss was carried out with aims at providing a clear reference of what is a good aspect ratio (or range of) to consider when designing a packed bed for utility-scale applications. The study considers a 24 hour long work cycle (12 hr charge + 12 hr discharge) with a 10 MW peak power and a total energy storage requirement of 79.4 MWh_{th} (or 33.4 MWh of exergy).

It has been found that for the duty analysed a substantial reduction in the total exergy losses of the packed bed can be attained by adopting a configuration based on an aspect ratio between 0.5 and 0.8 (the exact value depends on the value of β used). The improvement in performance is owed primarily to an increase in the surface area of rocks which narrows the temperature difference between the air and rocks reducing exergy losses due to heat transfer. In addition to this, the pumping load is lessened due to a decrement of the mass flux (ratio between mass flow of air /cross-sectional area) as the aspect ratio reduces.

It is important to note that, despite the overall reduction of exergy losses, exergy losses due to the self-discharge effect are far from negligible for designs based on a small aspect ratio ($\alpha \leq 0.5$). Consequently, designs based on a small aspect ratio are not particularly well suited for storage of exergy over extended periods of time, namely monthly or seasonal storage.

The optimization work undertaken has also explored the effect of the mass overrating factor (β), which is a factor that allows increasing the storage mass over the minimum amount required to improve the performance of the store. For instance, a packed bed with a β=1 has a roundtrip exergy efficiency of 95.1% (with the correct α and particle size) while this increases to 98.7% for a β=2 and to 99% for designs based on a β=3. Results seem to suggest that a store should be as big as possible to improve its efficiency; nevertheless, the factor by which the thermal mass of the store can be overrated is limited by economics. The improvement in performance becomes smaller for large values of β, which means that the additional capital expenditure associated with enlarging the store for a certain duty is not justified by the gains in efficiency obtained.

The cost-benefit analysis carried out shows that for the economic scenario considered (costs of materials, value per unit of exergy stored and lifespan of the plant) designs based on a β=3, yield the lowest profit due to their elevated CAPEX notwithstanding having the highest efficiencies. Analogously, designs based on a β=1, generate a very low profit due to their

comparatively high exergy losses despite having the lowest CAPEX.

For the work cycle considered, a packed bed with a β=1.5, an α=0.6 and with 4mm diameter rocks was found to be the optimum configuration, achieving a roundtrip efficiency of 98.24% and a levelized cost of storage of 68.2 $/MWh.

Acknowledgements

This research work has been carried out within the framework of the NexGen-TEST project; which has been made possible by a collaborative research initiative between the UK Engineering and Physical Sciences Research Council (EPSRC) and the National Natural Science Foundation of China (NSFC).

References

[1] S.D. Garvey, P.C. Eames. J.H. Wang, A.J. Pimm, M. Waterson, R.S. MacKay, M. Giulietti, L.C. Flatley, M. Thomson, J. Barton, D.J. Evans, J. Busby, J.E. Garvey. On generation-integrated energy storage. Energy Policy 2015; 86:544-551.

[2]M. Liu, N.H. S. Tay, S. Bell, M. Belusko, R. Jacob, G. Will, W.Saman, F. Bruno. Review on concentrating solar power plants and new developments in high temperature thermal energy storage technologies. Renewable and Sustainable Energy Reviews 2016; 53: 1411-1432.

[3] A. Gil, M. Medarno, I. Martorell, A. Lazaro, P. Dolado, B. Zalba, L.F. Cabeza. State of the art on high temperature thermal energy storage for power generation. Part 1: Concepts, materials and modellization. Renewable and Sustainable Energy Reviews 2010; 14: 31-35.

[4] S. Kuravi, J. Trahan, D.Y. Goswami, M.M. Rahman, E.K. Stefanakos. Thermal energy storage technologies and systems for concentrating solar power plants. Progress in Energy and Combustion Science 2013; 39:285-319.

[5] M. Budt, D. Wolf, R. Span, J. Yan. A review on compressed air energy storage: Basic principles, past milestones and recent developments. Applied Energy 2016; 170: 250-268.

[6] S.D. Garvey, A.J. Pimm (2016). Compressed air energy storage. In T. Letcher (Ed.), Storing energy (pp.87-111). Oxford, UK. Elsevier.

[7] E. Barbour, D. Mignard, Y.Ding, Y.Li. Adiabatic compressed air energy storage with packed bed thermal energy storage. Applied Energy 2015; 155:804-815.

[8] R. Bayón, E. Rojas. Simulation of thermocline storage for solar thermal power plants: from dimensionless results to prototypes and real-size tanks. Int J Heat Mass Transf 2013; 60:713–21.

[9]A. Modi, C.D. Pérez-Segarra. Thermocline thermal storage systems for concentrated solar power plants: one-dimensional numerical model and comparative analysis. Sol Energy 2014; 100:84–93.

[10] J.T. Van Lew, P. Li, C.L. Chan, W. Karaki, J. Stephens. Analysis of heat storage and delivery of a thermocline tank having solid filler material. J Sol Energy Eng, 2011; 021003-1:10.

[11]P. Li, J.T. Van Lew, W. Karaki, C.L. Chan, J. Stephens, Q. Wang. Generalized charts of energy storage effectiveness for thermocline heat storage tank design and calibration. Sol Energy 2011; 85:2130–43.

[12] C. Xu, X. Li, Z. Wang, Y. He, F. Bai. Effects of solid particle properties on the thermal performance of a packed-bed molten-salt thermocline thermal storage system. Appl Therm Eng 2013; 57:69–80.

[13] C. Xu, Z. Wang, Y. He, X. Li, F. Bai. Parametric study and standby behaviour of a packed-bed molten salt thermocline thermal storage system. Renewable Energy 2012; 48:1–9.

[14] Z. Yang, S.V. Garimella. Thermal analysis of solar thermal energy storage in a molten-salt thermocline. Sol Energy 2010; 84:974–85.

[15] Z. Yang, S.V. Garimella. Cyclic operation of molten-salt thermal energy storage in thermoclines for solar power plants. Appl Energy 2013; 103:256–65.

[16] M. Hänchen, S. Brückner, A. Steinfeld. High-temperature thermal storage using a packed bed of rocks- Heat transfer analysis and experimental validation. Appl Therm Eng 2011; 31:1798-1806.

[17] R. Anderson, L. Bates, E. Johnson, J.F. Morris. Packed bed thermal energy storage: A simplified experimentally validated model. Journal of Energy Storage 2015; 4:14–23.

[18] R. Anderson, S. Shiri, H. Bindra, J.F. Morris. Experimental results and modeling of energy storage and recovery in a packed bed of alumina particles, Appl. Energy 2014; 119:521-529.

[19] G. Zanganeh, A. Pedretti, S. Zavattoni, M. Barbato, A. Steinfeld. Packed-bed thermal storage for concentrated solar power – Pilot-scale demonstration and industrial-scale design. Solar Energy 2012; 86:3084-98.

[20] G. Zanganeh, A. Pedretti, S.A. Zavattoni, M.C. Barbato, A. Haselbacher, A. Steinfeld. Design of a 100 MWhth packed-bed thermal energy storage. Energy Procedia 2014; 49: 1071-1077.

[21] G. Zanganeh, A. Pedretti, A. Haselbacher, A. Steinfeld. Design of packed bed thermal energy storage systems for high-temperature industrial process heat. Applied Energy 2015; 137: 812–822.

[22] F. Opitz, P. Treffinger. Packed bed thermal energy storage model – Generalized approach and experimental validation. Appl Therm Eng 2014; 73:245-252.

[23] N.Mertens, F.Alobaid,L.Frigge,B.Epple. Dynamic simulation of integrated rock-bed thermocline storage for concentrated solar power. Solar Energy. 2014; 110:830-842.

[24] P. Klein, T.H. Roos, T.J. Sheer. Experimental investigation into a packed bed thermal storage solution for solar gas turbine systems. Energy Procedia 2014; 49: 840 – 849.

[25] P. Klein, T.H. Roos, T.J. Sheer. Parametric analysis of a high temperature packed bed thermal storage design for a solar gas turbine. Solar Energy 2015; 118:59–73.

[26] H. Agalit, N. Zari, M. Maalmi, M. Maaroufi. Numerical investigations of high temperature packed bed TES systems used in hybrid solar tower power plants. Solar Energy 2015; 122: 603–616.

[27] M. Medrano, A. Gil, I. Martorell, X. Potau, L.F. Cabeza. State of the art on high-temperature thermal energy storage for power generation. Part 2: Case studies Renewable and Sustainable Energy Reviews 2010; 14: 56–72.

[28] S.Zunft. Adiabatic CAES: The ADELE-ING project. Presented in: SCCER Heat & Electricity Storage Symposium. Villigen, Switzerland, May, 2015.

[29] A. Felix Regin, S.C. Solanki, J.S. Saini. An analysis of a packed bed latent heat thermal energy storage system using PCM capsules: Numerical investigation. Renewable energy 2009; 34:1765-1773.

[30] R. Singh, R.P. Sini, J.S. Saini. Nusselt number and friction factor correlations for packed bed solar energy storage system having large sized elements of different shapes. Solar energy 2006; 80:760-771.

[31] K.G. Allen, T.W. Backström, D.G. Kröger. Rock bed pressure drop and heat transfer: Simple design correlations. Solar energy 2015; 115:525-536

[32] K.G. Allen, T.W. Backström, D.G. Kröger. Packed rock bed thermal storage in power plants: design considerations. Energy Procedia 2014; 49:666-675

[33] S. Ergun. Fluid flow through paced columns. Chemical Engineering Progress 1952; 48:89-94.

[34] K.G. Allen, T.W. Backström, D.G. Kröger. Packed bed pressure drop dependence on particle shape, size distribution, packing arrangements and roughness. Powder Technology 2013; 246:590-600.

[35] R.E. Hicks. Pressure drop in packed beds of spheres. Industrial and Engineering Chemistry Fundamentals 1970; 9: 500-502.

[36] A. Montillet, Flow through a finite packed bed of spheres: a note on the limit of applicability of the Forchheimer-type equation, ASME Journal of Fluids Engineering 2004; 126:139–143.
[37] A. Montillet, E. Akkari, J. Comiti. About a correlating equation for predicting pressure drops through a packed bed of spheres in a large range of Reynolds numbers. Chemical Engineering and Processing 2007; 46:329–333.
[38] J. Trahan, A. Graziani, D.Y. Goswami, E. Stefanakos, C. Jotshi, N. Goel. Evaluation of pressure drop and particle sphericity for an air-rock bed thermal energy storage system. Energy Procedia 2014; 57:633-642.
[39] M. Cascetta, G. Cau, P. Puddu, F. Serra. A study of a packed bed thermal Energy Storage device: test rig, experimental and numerical results. Energy Procedia 2015; 81:987-994.
[40]A. White, G. Parks, C. Markides. Thermodynamic analysis of pumped thermal electricity storage. Applied thermal engineering 2013; 53:291-298
[41] T.R. Davenne, S.D. Garvey, B. Cardenas, M.C. Simpson. The cold store for a pumped thermal energy storage system. Journal of Energy Storage 2017; 14:295-310.
[42] E.W. Lemmon, R.T. Jacobsen. Viscosity and thermal conductivity equations for nitrogen, oxygen, argon and air, Int. J. Thermophys. 2004; 25:21–69.
[43] E.W. Lemmon, R.T. Jacobsen, S.G. Penoncello, D.G. Friend. Thermodynamic properties of air and mixtures of nitrogen, argon and oxygen from 60 to 2000 K at pressures to 2000 MPa, J. Phys. Chem. Ref. Data 2000; 29: 331–385.
[44] D.W. Waples, J.S. Waples. A review and evaluation of specific heat capacities of rocks, minerals and subsurface Fluids. Part 1; Minerals and Nonporous Rocks. Natural Resources Research 2004; 13:97-122
[45] K.G. Allen, T.W. Backström, D.G. Kröger, A.F.M. Kisters. Rock bed storage for solar thermal power plants: Rock characteristics, suitability, and availability. Solar Energy Materials & Solar Cells 2014; 126:170-183
[46] P. Hartlieb, M. Toifl, F. Kuchar, R. Meisels, T. Antretter. Thermo-physical properties of selected hard rocks and their relation to microwave assisted comminution. Minerals Engineering 2016; 91:34-41
[47] E. Weisstein. Sphere packing. From *MathWorld*: A Wolfram Web Resource. Available online at: http://mathworld.wolfram.com/SpherePacking.html
[48] V. Julch. Comparison of electricity storage options using levelized cost of storage (LCOS) method, Appl. Energy 2016; 183: 1594–1606
[49] M. Obi, S.M. Jensen, J.B. Ferris, R.B. Bass, Calculation of levelized costs of electricity for various electrical energy storage systems, Renew. Sustain. Energy Rev.2017; 67: 908–920.